Modelling of austenite stability in low-alloy triple-phase steels

Gregory N. Haidemenopoulos and Apostolos N. Vasilakos

A model for the stability of dispersed austenite in low alloy triple-phase steels has been developed. The model was based on the dislocation dissociation model for classical heterogeneous martensitic nucleation by considering stress effects on the nucleation site potency distribution. The driving force for martensitic transformation has been calculated with the aid of computational thermodynamics. The model allows for the effects of chemical composition of austenite, mean austenite particle size, yield strength of the steel and stress state on austenite stability. Chemical enrichment in C and Mn, as well as size refinement of the austenite particles lead to stabilization. On the contrary, the increase in the yield strength of the steel and triaxiality of the stress state lead to destabilization. The model can be used to determine the microstructural characteristics of the austenite dispersion, i.e. chemical composition and size, for optimum transformation plasticity interactions at the particular stress state of interest and can then be useful in the design of low-alloy triple-phase steels.

Modellierung der Austenitstabilität in niedriglegierten Dreiphasenstählen. Für die Stabilität des ausgeschiedenen Austenits in niedriglegierten Dreiphasenstählen wurde ein Modell entwickelt. Es basiert auf dem Modell der Versetzungsaufspaltung für die klassische heterogene Martensitkeimbildung unter Berücksichtigung des Spannungseinflusses auf die Keimstellenverteilung. Die treibende Kraft für die Martensitumwandlung wurde thermodynamisch berechnet. Das Modell berücksichtigt den Einfluß der chemischen Zusammensetzung des Austenits, der Austenitpartikelgröße, der Streckgrenze und des Spannungszustands auf die Austenitstabilität. Die Anreicherung an C und Mn und eine Austenitkornfeinung wirken stabilisierend. Im Gegensatz dazu führen der Streckgrenzenanstieg und der dreiachsige Spannungszustand zur einer Destabilisierung. Das Modell eignet sich zur Beschreibung der Gefügecharakteristika von Austenitausscheidungen -chemische Zusammensetzung und Teilchengröße-, die die für den jeweiligen Spannungszustand optimale Umwandlungsplastizität bewirken. Somit kann es hilfreich bei der Entwicklung von niedriglegierten Dreiphasenstählen sein.

Improvements in ductility and formability due to transformation induced plasticity (TRIP), are being currently exploited in low alloy steels for deep drawing or stretching applications. The microstructure of these so-called triple-phase steels consists of mixtures of ferrite/bainite/austenite or ferrite/martensite/austenite, where the austenite is present as a particle dispersion. It has been recognized that the most important parameter, which controls the TRIP interactions of dispersed austenite is its thermodynamic stability. Work has been focused in achieving austenite stabilization either by bainite transformation [1...3] or by direct cementite conversion during intercritical annealing [4...6].

This work is concerned with the modelling of the stability of austenitic dispersions in low alloy Fe-C-Mn-Si triple-phase steels. The aim of the model is twofold, i.e.:

- to identify and quantitatively determine the effect of austenite chemical composition and size, as well as strength and stress state on the stability of dispersed austenite and consequently on TRIP behaviour,
- to determine the austenite related microstructural parameters (chemical composition and size) that will tune its stability for optimum TRIP interactions for the stress state associated with a particular forming application.

Development of the model

Stability parameter. It has been chosen in this work to characterize the stability of dispersed austenite against mechanically induced transformation by a single parameter, the M_s^σ temperature, as the M_s temperature is used to characterize the stability of austenite against transformation on cooling. The M_s^σ temperature can be conveniently defined by considering mechanically induced martensitic transformation.

Deformation can stimulate the kinetics of solid-state phase transformations through both the thermodynamic effect of the applied stress and the production of new catalyzing defects by plastic strain. For the case of martensitic transformations, these interactions are depicted in **figure 1** [7]. Spontaneous transformation triggered by pre-existing nucleation sites occurs on cooling to the M_s

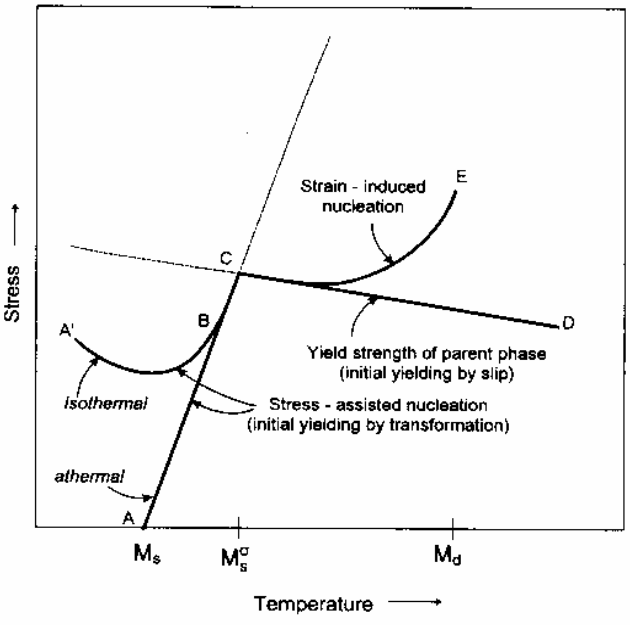

Figure 1. Schematic representation of stress assisted and strain induced regimes of mechanically induced martensitic transformation and definition of the M_s^σ temperature

Assistant Professor Dr.-Ing. Gregory Haidemenopoulos, Department of Mechanical and Industrial Engineering; *Dipl.-Ing. Apostolos Vasilakos*, University of Thessaly, Volos, Greece.

temperature (point A). Stress assisted nucleation on the same sites will occur at the stress denoted by the solid line indicated. At a temperature designated M_s^σ, this stress reaches the yield stress for slip in the parent phase (point C). Above M_s^σ new potent nucleation sites, introduced by the plastic strain, trigger strain induced nucleation (line CE). The temperature M_s^σ thus defines an approximate boundary between the temperature regimes where separate modes of the transformation dominate; near the M_s^σ temperature both modes will operate. Due to transformation plasticity, the observed yield stress follows the stress for stress assisted transformation below the M_s^σ (line CA for athermal and line CA' for isothermal martensitic transformation).

A reversal in the temperature dependence of the flow stress thus provides a convenient determination of the M_s^σ temperature. The M_s^σ temperature is then a quantitative characterization of the stability against stress assisted transformation. M_d is the maximum temperature above which martensitic transformation cannot be induced by deformation. Due to the interaction between stress triaxiality and transformation volume change, the M_s^σ and M_d temperatures are stress-state dependent.

For the case of austenite dispersions in Fe-C-Mn-Si alloys, the M_s^σ temperature depends on the following factors:

- chemical composition of the austenite particles (affects the chemical driving force for the martensitic transformation);
- austenite particle size (affects the probability of finding nucleation sites in the particle);
- stress state (due to the interaction of the transformational volume change with stress triaxiality);
- strength of the matrix (affects the mechanical driving force contribution to the total driving force for the martensitic transformation);

In the next paragraph, a functional form is derived, which links the above-mentioned factors to the M_s^σ temperature.

Transformation stress. For the case of stress assisted nucleation, the applied elastic stress assists the transformation kinetics by modifying the effective potency distribution of the pre-existing nucleation sites.

In order to describe the potency distribution of nucleation sites, reference should be made to the model of martensitic nucleation adopted in this work. According to Olson and Cohen [8], heterogeneous martensitic nucleation can proceed by the dissociation of an existing defect, which plays the role of the nucleation site for the transformation. This defect has the form of a dislocation array, which resides on an existing grain boundary or interphase boundary. The dissociation of such a defect produces a fault structure or martensite embryo, the growth of which depends on the energetics of the dissociation. The fault energy $\gamma_f(n)$ per unit area of a fault with a thickness of n planes can be expressed by:

$$\gamma_f(n) = n\rho\left[\Delta G^{ch} + E^{str} + W_f\right] + 2\gamma_s \qquad (1)$$

where ΔG^{ch} is the chemical driving force for martensitic transformation per unit volume, γ_s is the specific fault/matrix interfacial energy, ρ is the density of atoms in the fault plane, E^{str} is the elastic strain energy per unit volume associated with distortions in the fault interface plane, and W_f is the frictional work of the interfacial motion, which occurs during the dissociation process. For list of symbols, see **table 1.**

Spontaneous martensitic nucleation by the defect dissociation process described above can occur when $\gamma_f(n) \leq 0$. In this case the dissociation is barrierless, and occurs at a critical value of the chemical driving force ΔG^{ch} (or temperature).

Based on the above model, the potency of a nucleation site (defect) can be expressed in terms of the thickness n (in numbers of crystal planes) of the nucleus that can be derived from the defect by barrierless dissociation. The critical n for nucleation at a given thermodynamic driving force per unit volume ΔG^{ch} is according to equation (1):

$$n = -\frac{2\cdot\gamma_s/\rho}{\Delta G^{ch} + E^{str} + W_f}. \qquad (2)$$

Based on this model, Cohen and Olson [9] derived the cumulative structural defect-potency distribution from the Cech and Turnbull small-particle experiments in Fe-30Ni [10]. It was found, in these experiments, that martensitic nucleation in small particles, which were cooled from a high temperature, depends on the size of the particles. If a number density N_V of nucleation sites is randomly distributed throughout the volume, then the Cech-Turnbull experimental results, i.e. the fraction of particles which transform to martensite at a given temperature, define the value of $N_V(n)$ for sites of sufficient potency n to nucleate the

Table 1. List of symbols

n	potency of nucleation site for martensitic transformation
ΔG^{ch}	chemical driving force for martensitic transformation
γ_s	martensitic nucleus specific interfacial energy
ρ	density of atoms in close-packed plane
E^{str}	elastic strain energy associated with distortions in the nucleus
W_f	frictional work of interfacial motion
$N_V(n)$	cumulative structural defect potency distribution
N_V^0	total number of nucleation sites of all potencies
ΔG^σ	mechanical driving force for martensitic transformation
V_p	mean austenite particle volume
f	fraction of particles transformed
σ_t	transformation stress
σ_Y	yield strength
X_C	mole fraction carbon in austenite
X_{Mn}	mole fraction manganese in austenite
$(\sigma_h/\bar{\sigma})$	stress state parameter (ratio of hydrostatic to equivalent stress)

martensitic transformation on cooling to that given temperature. The cumulative structural defect potency distribution is then given by the following equation:

$$N_v = N_v^0 \exp(-\alpha \cdot n) \tag{3}$$

where N_v^0 is the total number of nucleation sites of all potencies and α is a constant.

The form of equation (2) is typical of experimentally observed distribution functions for sparsely distributed defects as encountered in fracture and fatigue.

The effect of the applied stress on the potency distribution can be found by adding a mechanical driving force term ΔG^{σ} to the chemical driving force term ΔG^{ch} of equation (2), to obtain the total thermodynamic driving force:

$$\Delta G = \Delta G_{ch} + \Delta G_{\sigma} \tag{4}$$

At a given stress level, the value of ΔG^{σ} changes with the orientation of the nucleus relative to the stress axis. The mechanical driving force due to a uniaxial elastic stress σ is then expressed as:

$$\Delta G^{\sigma} = \frac{\sigma}{2}\left\{\gamma_0 \cdot sin(2\theta) \cdot cos\beta + \varepsilon_0 \cdot \left(1 + cos(2\theta)\right)\right\} \tag{5}$$

where γ_0 and ε_0 are the transformation shear and normal strains, θ is the angle between the applied stress axis and the normal to the habit plane, and β is the angle between the shear direction of the transformation and the maximum shear direction of the applied stress resolved on the habit plane.

In considering stress effects on the potency distribution, two limiting cases should be considered. A fully-biased distribution which is based on the assumption by Patel and Cohen [11] that the operative nucleation sites are of the optimum orientation for maximum interaction with the applied stress, such that

$$\Delta G^{\sigma} = \Delta G^{\sigma}_{max}$$

for all sites. An opposite extreme is to consider a fully-random distribution, based on the assumption made by Olson, Tsuzaki, and Cohen [12] that the nucleation sites are randomly oriented. Olson, Tsuzaki, and Cohen found that in the stress assisted regime the effect of the applied stress is approximately one third of that predicted by the fully-biased distribution model. The actual behaviour should be bounded between these two extremes. Therefore, the potency distribution of nucleation sites $N_v(\sigma)$, under an applied elastic stress σ, is given by the following expression:

$$N_v(\sigma) = N_v^0 \exp\frac{2\alpha\gamma_s/\rho}{\Delta G^{ch} + \Delta G^{\sigma}_{max} + E^{str} + W_f} \tag{6}$$

where for the fully-random distribution of nucleation sites, the term ΔG^{σ}_{max} should be replaced by $\Delta G^{\sigma}_{max}/3$.

The mechanical driving force is related to the applied stress through the expression:

$$\Delta G^{\sigma} = \sigma\left(\frac{\partial \Delta G}{\partial \sigma}\right). \tag{7}$$

The stress assisted transformation of a well-spaced dispersion of metastable particles in a stable matrix is controlled by the pre-existing nucleation sites for which the potency distribution under an applied elastic stress σ is given by equation (6). For an average particle volume V_p, the fraction of particles, f, to transform via sites of a potency with a cumulative number density N_v is equal to the probability of finding at least one nucleation site in the particle, assuming that a single nucleation event transforms the particle to martensite. This probability is:

$$f = 1 - \exp\left(-N_v \cdot V_p\right). \tag{8}$$

The form of equation (8) is in agreement with the experimental results of Cech and Turnbull [10] mentioned earlier.

The transformation stress $\sigma = \sigma_t$, at which the martensitic nucleation is triggered, can then be found by combining equations (6), (7) and (8):

$$\sigma_t = \frac{1}{\left(\frac{\partial \Delta G}{\partial \sigma}\right)} \cdot \left\{ \frac{2\alpha\gamma_s/\rho}{\ln\left[-\frac{\ln(1-f)}{N_v^0 \cdot V_p}\right]} - \Delta G^{ch} - E^{str} - W_f \right\}. \tag{9}$$

The M_s^{σ} temperature can then be found by letting the transformation stress be equal to the yield strength ($\sigma_t = \sigma_y$) in the above equation and solve for the temperature, since the ΔG^{ch} term is temperature dependent. Before performing this operation, the individual terms in the above equation will be further developed.

Chemical driving force term. The chemical driving force for the martensitic transformation of austenite particles in Fe-C-Mn-Si alloys is a function of chemical composition and temperature, i.e.

$$\Delta G^{ch} = F(X_C, X_{Mn}, T) \tag{10}$$

where F denotes a function, X_C and X_{Mn} are the mole fractions of carbon and manganese in austenite respectively, and T is the temperature.

The effect of Si on austenite stability is not taken into account, since C and Mn are the most potential austenite stabilizing solutes. The chemical driving force for martensitic transformation is

$$\Delta G^{ch} = G(bcc) - G(fcc) \tag{11}$$

where G(bcc) and G(fcc) are the free energies of bcc and fcc phases of the same composition. The driving force

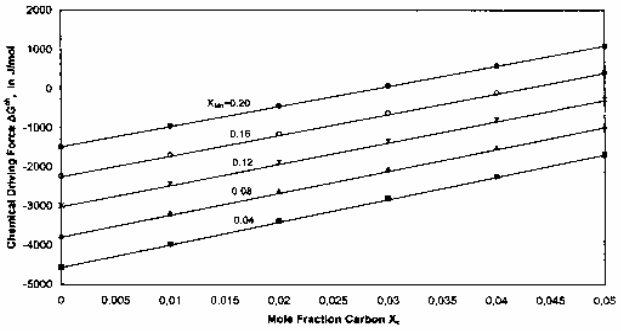

Figure 2. Chemical driving force for martensitic transformation, ΔG^{ch}, as a function of mole fraction C and Mn in austenite. Points are calculated values from Thermo-Calc, while lines represent a linear fit

ΔG^{ch} has been calculated, using the Thermo-Calc computational thermodynamics program [13] and employing the SGTE solution database (SGTE - Scientific Group Thermodata Europe).

In Thermo-Calc, the free energies of solution phases are described by the sub-lattice model, which was developed by Hillert and Staffanson [14] based on Temkin's model for ionic solutions [15] and extended by Sundman and Agren [16].

The calculations were carried out for $X_C = 0$ to 0.05 and $X_{Mn} = 0$ to 0.20.

The results of the calculation appear as points in **figure 2**. A linear curve-fitting procedure of the above data gives the expression for ΔG^{ch}, in J/Mol, as follows:

$$\Delta G^{ch} = -7381.6 + 69447 X_C + 19296 X_{Mn} - 38776 X_C X_{Mn} + 6.7821 T - 33.45 X_C T. \quad (12)$$

The above equation is also plotted (solid lines) in figure 2. The austenite stabilizing effects of both carbon and manganese are expressed by the increase of ΔG^{ch} to more positive values, the most potential austenite stabilizer being carbon.

Mechanical driving force contribution. The mechanical driving force contribution ΔG^{σ} defined in equation (7) is stress state dependent due to the interaction of the applied stress field with the transformation volume change.

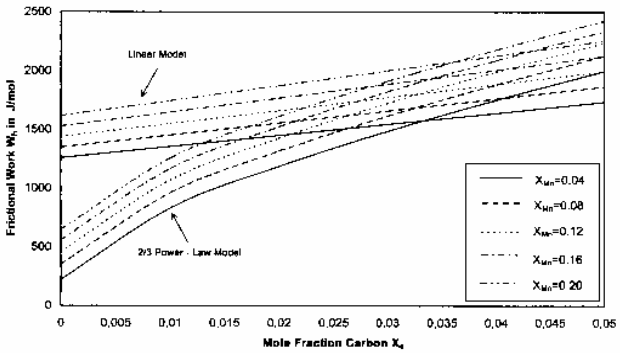

Figure 3. Frictional work of interfacial motion, W_f, as a function of mole fraction C and Mn in austenite. The two families of curves correspond to the linear and 2/3 power law approximations respectively

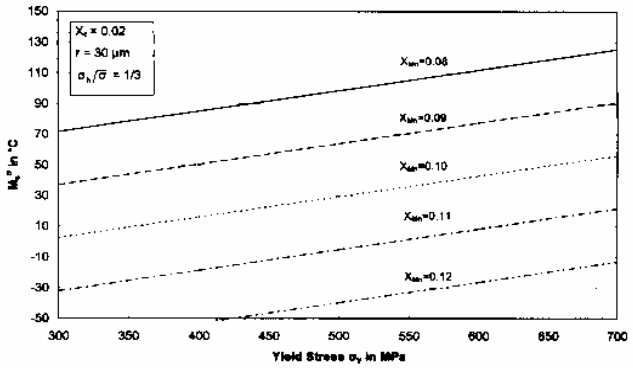

Figure 4. M_s^{σ} temperature as a function of yield strength for a range of manganese mole fraction in austenite

The parameter $(\partial \Delta G / \partial \sigma)$ in equation (7) is given as a function of stress state by Olson and Cohen [17] as follows: for compression -0.58 J/mol MPa, for tension -0.86 J/mol MPa and for the crack-tip -1.42 J/mol MPa. If the stress-state is represented by the parameter $(\sigma_h/\bar{\sigma})$ where σ_h is the hydrostatic stress and $\bar{\sigma}$ is the equivalent stress, then a straight line fit of the above data gives:

$$\frac{\partial \Delta G}{\partial \sigma} = -0.715 - 0.3206\left(\frac{\sigma_h}{\bar{\sigma}}\right) \quad (13)$$

where (σ_h/σ) = -1/3 for uniaxial compression, 0 for pure shear, and 1/3 for uniaxial tension.

Frictional work of interfacial motion. The frictional work of interfacial motion W_f in equation (9) is a function of chemical composition. Two ways have been followed in order to develop an expression of W_f.

The first way is to assume a linear increase of W_f with Mn and C content:

$$W_f = a_0 + a_1 X_C + a_2 X_{Mn} + a_3 X_C X_{Mn}. \quad (14)$$

In this case the frictional work is taken equal to the critical driving force at the M_s temperature. By adopting the data of Chang and Hsu [18] on the compositional dependence of the M_s temperature in Fe-C-Mn alloys, the following linear expression was obtained:

$$W_f = 1169 + 8777 X_C + 2246 X_{Mn} + 19900 X_C X_{Mn}. \quad (15)$$

The second approach is to follow the treatment of Labush [19] where the solution hardening effect is proportional to the 2/3 power of the alloying element. Again taking W_f as the critical driving force at M_s and adopting the data of Kuroda [20] for Fe-C-Mn alloys, the following 2/3 power-law expression was obtained (W_f in J/mol):

$$W_f = 1.893 \cdot 10^3 X_{Mn}^{2/3} + 1.310 \cdot 10^4 X_C^{2/3}. \quad (16)$$

Both expressions, equation (15) and equation (16) are plotted in **figure 3**. At low carbon contents, the discrep-

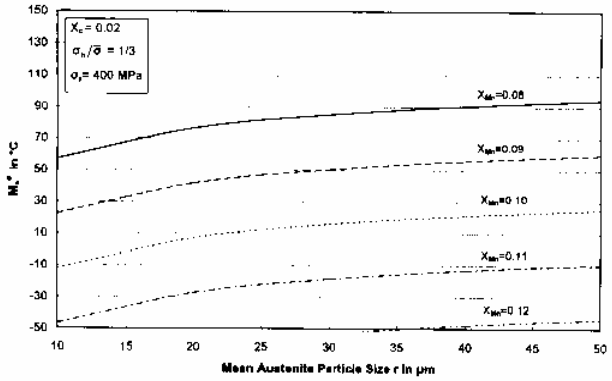

Figure 5. M_s^σ temperature as a function of mean austenite particle size for a range of manganese mole fraction in austenite

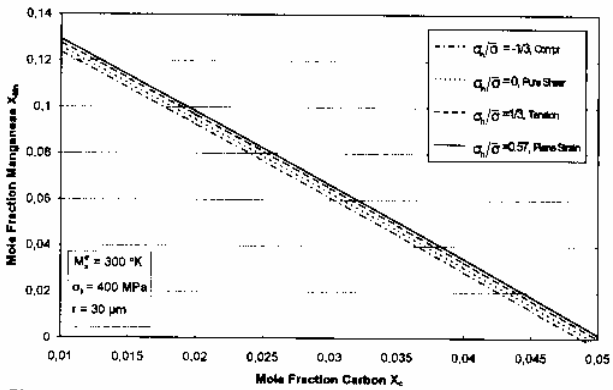

Figure 7. Required chemical composition of austenite in mole fraction manganese and mole fraction carbon for various stress state conditions and austenite stability at M_s^σ = 300 K

ancy between the linear and the 2/3 power-law model is large, approaching 1000 J/mol. This discrepancy almost vanishes for austenite carbon contents of X_C = 0.015 and above.

Calculation of the M_s^σ temperature

The M_s^σ temperature can be obtained if the expressions for the chemical driving force, equation (12), mechanical driving force, equation (13), and frictional work, equations (15)-(16), are inserted into the expression for the transformation stress, equation (9), and solve for the temperature.

The resulting expressions are the following:

for linear W_f model, equation (15)

$$M_s^\sigma = (6.7891 - 33.45 \cdot X_C)^{-1} \cdot \{A + 5712.6 - 78224 \cdot X_C - 21542 \cdot X_{Mn} + 18876 \cdot X_C \cdot X_{Mn} + \sigma_y \cdot \left(0.715 + 0.3206 \cdot \frac{\sigma_h}{\bar{\sigma}}\right)\}; \quad (17)$$

for the 2/3 power-law W_f model, equation (16)

$$M_s^\sigma = (6.7891 - 33.45 \cdot X_C)^{-1} \cdot (A + 6881.6 - 69447 \cdot X_C - 19296 \cdot X_{Mn} + 38776 \cdot X_C \cdot X_{Mn} - 1893 \cdot X_{Mn}^{2/3} - 13100 \cdot X_C^{2/3} + \sigma_y \cdot \left(0.715 + 0.3206 \cdot \frac{\sigma_h}{\bar{\sigma}}\right)) \quad (18)$$

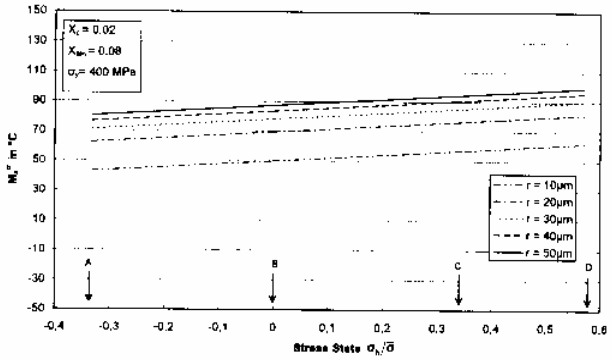

Figure 6. M_s^σ temperature as a function of stress state parameter for a range of carbon mole fraction in austenite. Arrows correspond to the stress states of uniaxial compression (A), pure shear (B), uniaxial tension (C) and plane strain tension (D)

where

$$A = \frac{2 \cdot \alpha \cdot \gamma_S / \rho}{\ln\left\{-\left[\ln(1-f)\right] / N_v^0 \cdot V_p\right\}}. \quad (19)$$

The values of the various parameters in the expression for A are the following:

$\alpha = 0.866$, $\gamma_S = 0.15$ J/m^2, $\rho = 3 \cdot 10^{-5}$ mol/m^2,

$f = 0.01$, $N_v^0 = 2 \cdot 10^{17}$ m^{-3}, $E^{str} = 500$ J/mol.

The austenite particle volume V_p has been replaced by the mean austenite particle radius r, assuming spherical particles for simplicity.

The calculations for the M_s^σ temperatures have been performed using the linear model for W_f. **Figure 4** shows calculated M_s^σ temperatures as a function of yield strength, for the range of Mn mole fraction in austenite from 0.08 to 0.12 and for particular mole fraction carbon, austenite particle radius and stress state (uniaxial tension). The M_s^σ temperature increases with the yield strength of the steel, indicating the de-stabilizing effect of the high yield strength. **Figure 5** shows calculated M_s^σ temperatures as a function of mean austenite particle radius, for the range of Mn mole fraction in austenite from 0.08 to 0.12 and for particular mole fraction carbon, yield strength and stress state (uniaxial tension). The M_s^σ temperature increases with austenite particle size, indicating the stabilizing effect of austenite particle size refinement. **Figure 6** shows calculated M_s^σ temperatures as a function of stress state, for the range of austenite particle sizes from 10 to 50 µm and for particular mole fraction carbon and manganese, and yield strength. The M_s^σ temperature increases with the stress state parameter $(\sigma_h/\bar{\sigma})$, indicating the destabilizing effect of triaxiality.

Microstructural requirements for optimum TRIP interactions

Enhanced mechanical behaviour, i.e. enhanced ductility and toughness is associated with the strain induced martensitic transformation of austenite. In particular, en-

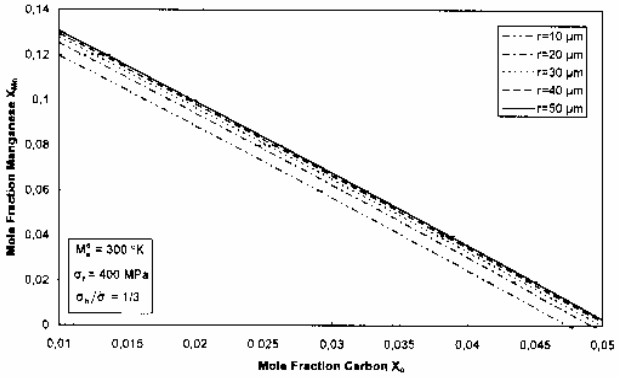

Figure 8. Required chemical composition of austenite in mole fraction manganese and mole fraction carbon for a range of mean austenite particle size and austenite stability at M_s^σ = 300 K

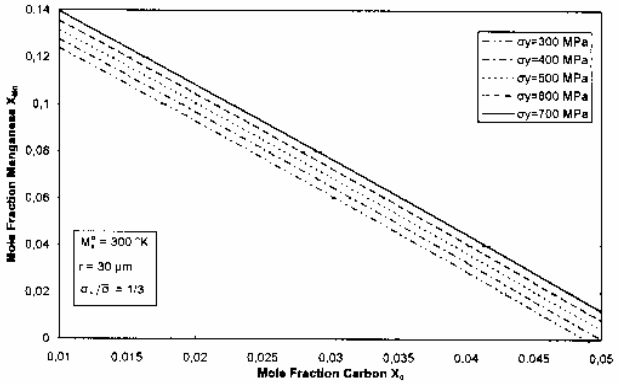

Figure 9. Required chemical composition of austenite in mole fraction manganese and mole fraction carbon for a range of yield strengths and austenite stability at M_s^σ = 300 K

hanced formability is associated with the flow stabilizing effect of transformation plasticity during strain induced transformation. This mode of transformation operates above the M_s^σ temperature for the stress state of interest. It has been determined experimentally [21] that for maximum property enhancement, the M_s^σ temperature should be just below the service temperature (e.g. room temperature). The model which was developed above can be used to determine the microstructural requirements, which should be satisfied by the austenitic dispersion, for optimum TRIP interactions. By setting M_s^σ = 300 K in equation (17), the relations between chemical enrichment and size refinement can be deduced. **Figure 7** shows the required chemical enrichment of austenite (in C and Mn) as a function of stress state. An increase in the triaxiality of the stress state (going from compression to tension and to plane strain tension), sets the requirement for significant chemical enrichment in carbon and manganese. For plane strain tension, encountered in deep drawing operations, the austenite dispersion should possess higher stability than that required for ductility enhancement in simple uniaxial tension.

Figure 8 shows the required chemical enrichment of austenite (in C and Mn) as a function of mean austenite particle size. This figure indicates that the coarser the austenite dispersion, the more chemically enriched it should be, in order to maintain the optimum stability level of M_s^σ = 300 K. Finally **figure 9** shows the required chemical enrichment of austenite (in C and Mn) as a function of yield strength. For the same stress state, an increase in the yield strength of the steel sets the requirement for significant chemical enrichment in order to maintain the stability of austenite particles at the optimum level of M_s^σ = 300 K.

Conclusions

From the calculated values of the M_s^σ temperature, the following comments regarding austenite stability can be made:

- the M_s^σ temperature increases and thus the austenite stability decreases as the yield stress is increased;
- the M_s^σ temperature increases (stability decrease) as the mean austenite particle size increases;
- the M_s^σ temperature increases (stability decrease) as the stress state parameter $(\sigma_h/\bar{\sigma})$ increases from -1/3 (for uniaxial compression) to 0 (for pure shear), to 1/3 (for uniaxial tension), to 0.57 (for plane strain tension);
- there is a strong chemical stabilization effect associated with C and Mn enrichment of the austenite particles;
- the model can be used to determine the microstructural requirements of the austenite dispersions (chemical composition and size) for mechanical property enhancement (ductility and formability) via TRIP interactions in low-alloy triple-phase steels.

Acknowledgement

This work has been partially supported by the European Commission through the project ECSC 7210-EC702-95-D3.03e.

(A 01 152; received: 26. January 1996;
in revised form: 09. April 1996)

References

[1] *Sakuma, Y.; Matsumura, O.; Takechi, H.*: Met. Trans. 22A (1991), p. 531/38.
[2] *Brandt, M.L.; Olson, G.B.*: Iron & Steelmaker 5 (1993), p. 55/60.
[3] *Haidemenopoulos, G.N.; Papadimitriou, K.*: steel res. 66 (1995), p. 433/38.
[4] U.S. Patent No. 4, 544, 422: Ferrite-Austenite Dual Phase Steel, October 1985.
[5] *Grujicic, M.; Buonanno, M.; Allen, S.M.; Olson, G.B.; Cohen, M.*: Heterogeneous Precipitation of Austenite for Stabilization. Proc. 34th Sagamore Army Materials Research Conf. on Innovations of Ultrahigh-Strength Steel Technology, [eds.:] Olson, G.B.; Azrin, M.; Wright, E.S., Lake George, NY, 1987, p. 527/47.
[6] *Haidemenopoulos, G.N.*: steel res. 67 (1996) No.3, p. 93/99.
[7] *Olson, G. B.*: Mechanically-Induced Phase Transformations in Alloys, Encyclopedia of Mat. Sci.and Eng., [ed.:] Bever, M.B., Pergamon Press, Cambridge, MA, 1986, p. 2929/32.
[8] *Olson, G. B.; Cohen, M.*: Met. Trans. 7A (1976), p. 1897.
[9] *Cohen, M.; Olson, G.B.*: Japan. Suppl. Trans. JIM 17 (1976), p. 93.

[10] *Cech, R.E.; Turnbull, D.*: Trans. AIME 206 (1956), p. 124.
[11] *Patel, J.R.; Cohen, M.*: Acta Metall. 1 (1953), p. 531.
[12] *Olson, G.B; Tsuzaki, K.; Cohen, M.*: MRS Proc. 57 (1987), p. 129/148.
[13] *Sundman ,B. ; Jansson, B., Anderson, J.-O.*: CALPHAD 9 (1985), p. 153.
[14] *Hillert, M.; Staffanson, L.-I.*: Acta Chem. Scand. 24 (1970), p. 3618/26.
[15] *Temkin, M.*: Acta Phys. Chim. 20 (1945), p. 411/20.
[16] *Sundman, B.; Agren, J.*: J. Phys. Chem. Solids 42M (1981), p. 297/301.
[17] *Olson, G.B.; Cohen, M.*: Met. Trans. 13A (1982), p. 1907.
[18] *Chang, H.; Hsu, T.Y.*: Acta Met. 34 (1986), p. 333/38.
[19] *Labush, R.*: J. Phys. Stat. Solid 41 (1970) p. 659/69.
[20] *Kuroda, Y.*: Kinetics of Deformation-Induced Transformation of Dispersed Austenite In Two Alloy Systems, Cambridge, MA ,1987 (S.M. thesis).
[21] *Leal, R. H.*: Transformation Toughening of Metastable Austenitic Steels, Cambridge, MA ,1984 (Ph.D. thesis).